

## Permeability and Diffusion through Mechanically Deformed Random Polymer Networks

Hassan Masoud and Alexander Alexeev\*

George W. Woodruff School of Mechanical Engineering, Georgia Institute of Technology, Atlanta, Georgia 30332, United States

Received September 3, 2010; Revised Manuscript Received October 19, 2010

**ABSTRACT:** We develop a hybrid computational method to examine the permeation and hindered diffusion through mechanically loaded (anisotropic) polymer networks. We use the bond-bending lattice spring model to capture the micromechanics of random networks of interconnected filaments coupled with the dissipative particle dynamics to explicitly model the viscous fluid and diffusive objects. Our simulations reveal that the transport properties are independent of the network internal organization and are solely function of the network porosity and degree of anisotropy due to a mechanical deformation. Furthermore, our results indicate that the network permeability under load can be estimated based on the network alignment that is characterized by a second order orientation tensor. Our findings have implications for designing drug delivery agents, paper manufacturing, tissue engineering, and understanding the function of biological systems.

### Introduction

Polymer networks are natural (e.g., cytoskeletal structures), synthetic (e.g., hydrogels), or hybrid natural-synthetic (e.g., PEGylated fibrinogen) materials in which constituting polymer chains are all connected to each other either directly or via other connecting chains.<sup>1</sup> These highly permeable, extremely flexible, and yet mechanically sturdy polymer materials have found many applications in today's state-of-the-art technologies.<sup>2–4</sup> In addition to their conventional use as structural (hydrophobic networks) and superabsorbent (hydrogels) materials, polymer networks are successfully employed in biotechnology and medicine,<sup>5</sup> as matrices for drug delivery,<sup>6,7</sup> scaffolds for tissue engineering,<sup>8</sup> materials for soft contact lenses<sup>9</sup> (silicone hydrogels) and breast implants.<sup>10</sup> Furthermore, stimuli-responsive polymer gels are used in robotics to build effective microactuators<sup>11</sup> and microrobots,<sup>12,13</sup> and to create different kinds of smart materials.<sup>14,15</sup>

The ever increasing importance of polymer networks requires an in-depth understanding of their properties. Indeed, using theory and experiment, researchers have extensively studied the transport properties, i.e., permeability and diffusivity, of filamentous networks.<sup>5,6,16–31</sup> Specifically, Phillips<sup>20,21</sup> introduced a hydrodynamic scaling model that is capable of describing most of the available experimental data. According to this model, diffusion of various types of objects in polymer networks is given by  $D/D_0 = \exp(-\alpha R^\delta \phi^\nu)$ , where  $D_0$  is the diffusion coefficient of the object in the absence of the polymer network,  $R$  represents a characteristic size of the object,  $\phi$  is the network volume fraction, and  $\nu$  and  $\delta$  are the scaling exponents. The exponent  $\nu$  was predicted to lie between 0.5 and 1. Recently, Seiffert and Oppermann<sup>27</sup> carried out a series of experiments and measured the diffusion of linear macromolecules and spherical particles in semidilute polymer solutions and polymer networks. They found, in contrast to the prediction of the Phillips model, that the diffusion of flexible polymers and rigid particles having a comparable size is not identical. Nevertheless, they indicated that the model provides a

reasonable fit to the individual data sets and reported values of  $\nu = 0.7$  and  $\nu = 0.8$  for the diffusion of solid particles and linear macromolecules, respectively. Similar to diffusivity, permeability of ordered and disordered fibrous networks has been extensively studied. Even though the results of different experiments are scattered, the data was found to follow a similar trend and agrees within an order of magnitude. A comprehensive review of experimental and theoretical permeability data is available elsewhere.<sup>18</sup>

In practical applications, polymer networks are often under mechanical deformation, which gives rise to changes in the filament orientation and also may alter the volume of the network. The change in filament orientation can affect the network transport properties.<sup>28,30,32</sup> It is, therefore, important to assess the effect of applied mechanical deformation on permeability and diffusivity of initially isotropic random polymer networks. Recently, the effects of axial compression on the permeability of articular cartilages, agarose gels<sup>24</sup> and deformable foams<sup>25</sup> were examined. It was found that, under confined compression/tension, permeability is a nonlinear function of applied strain and relatively insensitive to the changes in water volume fraction.

Herein, we set up a mesoscopic simulation model to study the permeation and diffusion through mechanically deformed random polymer networks. First, we study the permeability, self-diffusion, and particle/chain diffusion in unstressed (isotropic) random networks and examine the difference in hindered diffusion between rigid nanoparticles and soft polymer chains. We then probe the effect of compressive, tensile, and shearing stresses on the network transport properties.

### Methodology

We use dissipative particle dynamics (DPD)<sup>33,34</sup> to capture the complex interactions among a viscous fluid, diffusive objects, and a deformable polymer network. DPD is a coarse-grained simulation technique that employs a momentum-conserving thermostat and soft repulsive interactions among beads representing clusters of molecules. This allows for simulations of physical phenomena occurring at relatively large time and spatial scales, while accurately

\*Corresponding author. E-mail: alexander.alexeev@me.gatech.edu.

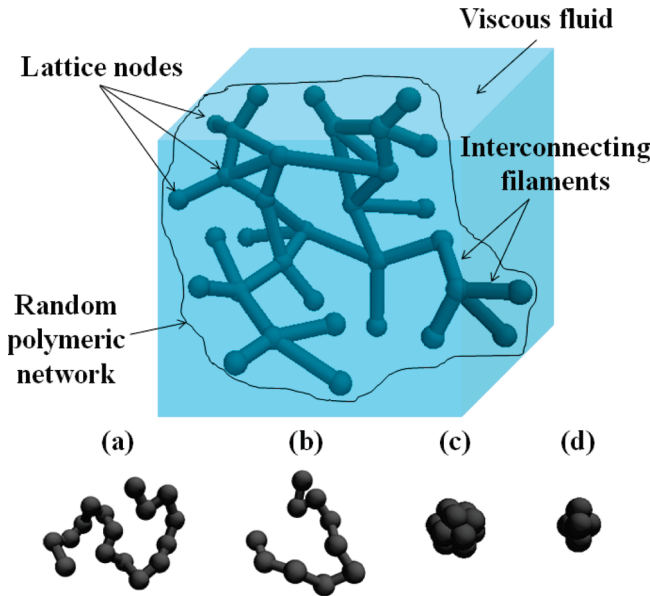


**Figure 1.** Schematic illustrating system components within a periodic simulation box. Insets a and b show 16-bead and 10-bead polymer chains, respectively. Insets c and d show, respectively, 13-bead and 5-bead hexagonal closed-packed aggregates representing nanoparticles.

capturing the relevant hydrodynamic effects. Indeed, DPD has been successfully employed in the dynamic simulations of polymers and particles dispersed in Newtonian incompressible fluids.<sup>35–39</sup>

In DPD, the time evolution of the many-body system obeys the Newton's second law  $m \frac{dv_i}{dt} = \mathbf{f}_i$ , where  $v_i$  and  $\mathbf{f}_i$  are, respectively, the velocity and force on a bead  $i$  with mass  $m$ , and  $t$  is time. The equations of motion are integrated using the velocity-Verlet algorithm.<sup>34</sup> The force on a bead is  $\mathbf{f}_i = \sum_j (\mathbf{F}_{ij}^C + \mathbf{F}_{ij}^D + \mathbf{F}_{ij}^R)$ , where the sum runs over all beads  $j$  within a cutoff radius  $r_c$  around the bead  $i$ . The conservative force is given by  $\mathbf{F}_{ij}^C = a_{ij}(1 - \hat{r}_{ij})\hat{\mathbf{r}}_{ij}$ , where  $a_{ij}$  is the repulsion between beads  $i$  and  $j$ ,  $\hat{r}_{ij} = r_{ij}/r_c$  and  $\hat{\mathbf{r}}_{ij} = \mathbf{r}_{ij}/r_{ij}$  with  $r_{ij} = |\mathbf{r}_i - \mathbf{r}_j|$ . The dissipative force is  $\mathbf{F}_{ij}^D = -\gamma \omega^D(r_{ij})(\hat{\mathbf{r}}_{ij} \cdot \mathbf{v}_{ij})\hat{\mathbf{r}}_{ij}$  and the random force is  $\mathbf{F}_{ij}^R = \sigma \omega^R(r_{ij})\xi_{ij}\hat{\mathbf{r}}_{ij} dt^{1/2}$ , where  $\mathbf{v}_{ij} = \mathbf{v}_i - \mathbf{v}_j$  and  $\xi_{ij}$  is a zero-mean Gaussian random variable of unit variance with  $\xi_{ji} = \xi_{ij}$ . The coefficients  $\gamma$  and  $\sigma^2 = 2k_B T \gamma$  determine the strength of dissipative and random forces, where  $k_B$  is the Boltzmann constant and  $T$  is the temperature of the system. Moreover, the weight functions  $\omega^D(r_{ij})$  and  $\omega^R(r_{ij})$  are related via  $\omega^D(r_{ij}) = [\omega^R(r_{ij})]^2$ . The relations between the weight functions and the strength of dissipative and random forces are set to ensure the thermodynamic equilibrium.<sup>40</sup> The generalized form of the weight function is given by  $\omega^R(r_{ij}) = (1 - \hat{r}_{ij})^p$  with  $p = 1$  for the standard DPD model.<sup>41</sup> In our simulations, we set the time step  $\Delta t = 0.01$ ,  $p = 1$ ,  $m = 1$ ,  $r_c = 1$ ,  $\gamma = 4.5$ ,  $a = 25$ ,  $k_B T = 1$  and the solvent number density  $\rho = 3$  yielding the solvent kinematic viscosity  $\nu$  equal to 0.283. Unless specified otherwise, all dimensional values are given in DPD units.

Our simulations are carried out in a periodic box that encompasses a viscous solvent, an elastic polymer network, and diffusive objects, such as polymer chains and rigid particles (Figure 1). The domain dimensions are  $10 \times 10 \times 10$  in the  $x$ ,  $y$ , and  $z$  directions, respectively. This is to ensure that the domain is greater than the minimum box size of  $14k^{1/2}$ , as suggested by Clague and Phillips<sup>22</sup> based on the Brinkman screening length criterion. Here,  $k$  is the network permeability.

Flexible polymers consist of either 10 or 16 DPD beads connected sequentially by finitely extensible nonlinear elastic (FENE) springs. The FENE potential is given by  $U_{\text{FENE}} = -0.5 k_s r_{\max}^2 \log[1 - |\mathbf{r}_i - \mathbf{r}_j|^2/r_{\max}^2]$ , where  $k_{\text{FENE}} = 10$  is the stretching constant and  $r_{\max} = 2$  is the maximum spring extension. The polymer

radii of gyration are, respectively,  $R_{g0} \approx 1$  and  $R_{g0} \approx 1.33$ , as calculated from the equilibrium simulations. Two types of rigid particles are constructed from 5 and 13 DPD beads arranged in hexagonal close-packed spherical aggregates that obey the rigid body dynamics and interact with solvent particles and polymer network (described below) via the DPD potential. The Stokes-Einstein radii of the aggregates are  $R_{SE} \approx 0.45$  and  $R_{SE} \approx 0.7$ , respectively.<sup>42</sup> It can be shown that the Stokes-Einstein radii at low Reynolds number correspond to the effective hydrodynamic radii of DPD particles and aggregates with no-slip boundaries.<sup>42</sup>

A random lattice of interconnecting elastic filaments is used to simulate a semiflexible polymer network that captures the mechanical properties of the disordered polymer networks.<sup>43</sup> The flexible filaments are formed from DPD particles connected by Frankel springs with a potential  $U_{\text{Frankel}} = -k_{\text{Frankel}} (|\mathbf{r}_i - \mathbf{r}_j| - r_{eq})^2/2$ . Here, we set the spring constant  $k_{\text{Frankel}} = 200$  and the equilibrium length  $r_{eq} = 0.418$ . Additionally, we include a bending potential  $U_b = k_b(1 + \cos \theta)$ , where  $k_b = 2.5$  is the bending stiffness and  $\theta$  is the angle between two consecutive pairs of beads. This leads to a filament bending rigidity equal to  $EI \approx 0.913$ , if we assume that the radius of filaments equals to the Stokes-Einstein radius of DPD beads,  $R_{SE} \approx 0.209$ .<sup>42</sup> We note that the number of beads  $n_f$  in a filament with the length of  $l_f$  is given by  $1 + l_f/r_{eq}$ .

We build the polymer network in two steps (Figure 1). We first randomly distribute  $N$  seed nodes inside the computational domain. Then, we connect each node with  $C_{ave}$  closest nodes that are located within a cutoff radius, which is set to prevent the formation of excessively long filaments. The resulting average network connectivity deviates from the value of  $C_{ave}$  by less than one percent. Thus, we construct polymer networks that are uniquely characterized by the number of lattice nodes  $N$  and the average connectivity  $C_{ave}$ . In this paper, we consider networks with  $N = 250$ ,  $500$ ,  $1000$  and  $C_{ave} = 4, 6, 8, 10, 12, 14$ .

When it comes to the analysis of transport properties of porous media, one of the main controlling parameters is the medium porosity. Here, we define the network porosity as  $\epsilon = 1 - V_{\text{filaments}}/V_{\text{box}}$ , where  $V_{\text{box}}$  is the total volume of the simulation domain and  $V_{\text{filaments}} = 4/3 n_{\text{total}} \pi R_{SE}^3$  is the volume occupied by the filaments in which  $n_{\text{total}}$  is the total number of DPD beads used to build the network ( $n_{\text{total}}$  is different from the number of lattice seed nodes  $N$ ). When we calculate the porosity some of the filaments may overlap, and thus, the resulting value exceeds the real network porosity by a few percent. Since the total number of filaments in the network is equal to  $N C_{ave}/2$  and the average filaments length varies proportionally to  $N^{-1/3}(C_{ave} + C_0)$ , where  $C_0$  is a constant related to the average distance between lattice nodes  $N^{-1/3}C_0$ , we can estimate the network porosity using the following equation  $\epsilon = 1 - N^{2/3} C_{ave} (a C_{ave} + b)$ . We find that for networks considered in our studies  $a = 1.18 \times 10^{-5}$  and  $b = 2.346 \times 10^{-4}$ . Parts a and b of Figure 2 show two networks constructed with different values of  $N$  and  $C_{ave}$ . Here, we choose the network parameters such that the porosity  $\epsilon$  is roughly 0.8 for both networks. As we show below, despite the notable difference in their internal structures, these networks exhibit similar transport properties.

To assess transport properties of the constructed polymer networks, we examine the permeability and diffusivity of unstressed networks and networks under mechanical load. In all cases, we first equilibrate the network without solvent, then fix the network geometry and introduce solvent. In permeability calculations, we apply an external body force  $\mathbf{F}_{\text{external}} = 0.01(\hat{\mathbf{e}}_x + \hat{\mathbf{e}}_y + \hat{\mathbf{e}}_z)$  to drive the fluid flow through the network. We run the simulations for  $3.2 \times 10^5$  time steps and evaluate the components of volume-averaged flow velocity,  $\langle \mathbf{u} \rangle$ , in the  $x$ ,  $y$ , and  $z$  directions. Next, we use Darcy's law  $k = \langle \mathbf{u} \rangle v/f$  to find the permeability in each direction.<sup>19</sup> Finally, we average the permeability results over symmetric directions within the network.

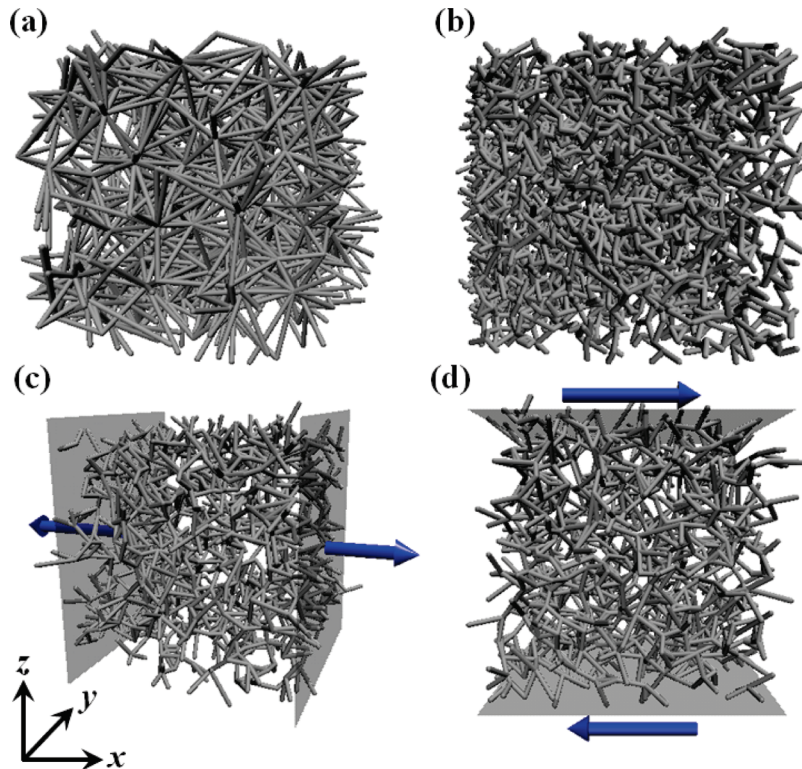


**Figure 2.** Networks with porosity  $\varepsilon = 0.8$  and different internal structures: (a)  $N = 2000$  and  $C_{ave} = 3$ ; (b)  $N = 250$  and  $C_{ave} = 12$ . Panels c and d show networks under normal and shear deformation, respectively. The arrows indicate the directions of applied forces.

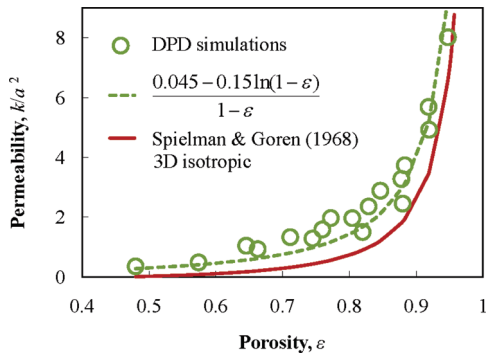


**Figure 3.** Permeability as a function of porosity in 3D isotropic random polymer networks. The network parameters are  $N = 250, 500, 1000$  and  $C_{ave} = 4, 6, 8, 10, 12, 14$ .

To evaluate network diffusivity, we introduce 30 diffusive objects (chains or particles) that are initially randomly distributed in solvent. We continue the simulations for  $8 \times 10^5$  time steps to collect sufficient statistics regarding the entities' diffusion. We then calculate the diffusion coefficients using the long-time, mean-square displacement (MSD) relation of Einstein  $D = C\langle|r(t) - r(0)|^2\rangle/t$ , where  $\langle\dots\rangle$  represents the ensemble average,  $C$  is a constant, and  $r(t) - r(0)$  is the object position at time  $t$  relative to its original position.

Below, we first describe how we validate our methodology by comparing our results for undeformed networks with the previously reported numerical and experimental data. We then explore how the transport properties change when networks undergo mechanical deformation.

### Model Validation

We validate our simulation method by calculating the permeability and diffusivity in unstressed networks with different  $N$  and

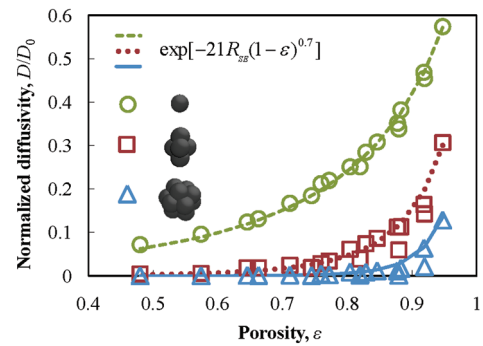


**Figure 4.** Diffusivity of solvent particles (self-diffusivity), and rigid particles of radii  $R_{SE} \approx 0.45$  and  $R_{SE} \approx 0.7$  in 3D isotropic random polymer networks as a function of network porosity. The network parameters are  $N = 250, 500, 1000$  and  $C_{ave} = 4, 6, 8, 10, 12, 14$ .

$C_{ave}$  (Figures 3, 4 and 5). The permeability is nondimensionalized by dividing it by the square of filament radius, which is equal to the Stokes–Einstein radius of a DPD particle. We find good agreement between our permeability–porosity results for networks with different  $N$  and  $C_{ave}$  and the results of Spielman and Goren<sup>16</sup> for isotropic porous media (Figure 3). Slightly higher permeability predicted by our model can be attributed to a somewhat lower drag on filaments constructed from spheres as compared to cylindrical filaments.<sup>44</sup> Figure 3 also demonstrates that the permeability of a random filament network depends solely on the network volume fraction and is not a function of the network internal structure. This is in agreement with previously reported results.<sup>31</sup>

Figures 4 presents the results of DPD simulation for hindered diffusion of solvent particles (self-diffusion) and rigid particles of radii  $R_{SE} \approx 0.45$  and  $R_{SE} \approx 0.7$ . The diffusion of 10- and 16-bead polymer chains with radii of gyration equal to  $R_{g0} \approx 0.97$  and  $R_{g0} \approx 1.33$ , respectively, is shown in Figure 5a. Similar to

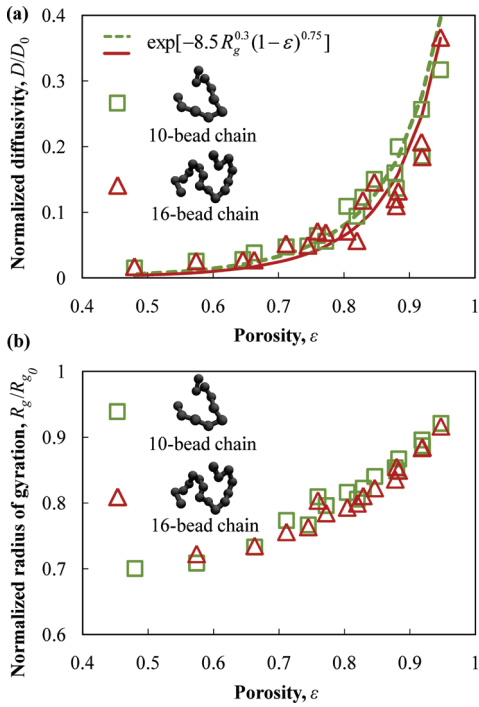


**Figure 5.** (a) Diffusivity and (b) gyration radius as a function of network porosity of 10 and 16-bead polymer chains in 3D isotropic random polymer networks. The network parameters are  $N = 250, 500, 1000$  and  $C_{ave} = 4, 6, 8, 10, 12, 14$ .

permeability data, the results are plotted versus network porosity for networks with different  $N$  and  $C_{ave}$ . Figures 4 and 5a show excellent agreement between our simulations and the experiments of Seiffert and Oppermann.<sup>27</sup>

We also find that the hydrodynamic scaling model<sup>20,21</sup> properly predicts the diffusion of rigid particles and linear macromolecules in random polymer networks. Our results are best fit by exponents  $\nu = 0.7$ ,  $\delta = 1$  and  $\nu = 0.75$ ,  $\delta = 0.3$  for solid particles and polymer chains, respectively. The smaller value of the scaling exponent  $\delta$  for chains indicates weaker dependence of the diffusion on the polymer radius of gyration (see Figure 4 and Figure 5a). Moreover, in agreement with previous studies,<sup>6,27</sup> our results show that the diffusion coefficient of solid particles is smaller than that of flexible polymers with a similar coil size. This is related to different mechanisms controlling diffusion of solid object and flexible polymers. Unlike solid particles that have a constant outer radius, the radius of gyration of polymeric chains changes when a chain diffuses through a network. Figure 5b illustrates that the radius of gyration decreases with decreasing the network porosity for greater  $\varepsilon$  and approaches a constant value as the network becomes denser. The reduction in chains' radius of gyration enhances their hindered diffusion in polymer networks and, therefore, yields greater diffusivity comparing to rigid particles.

## Results and Discussion

We are now able to discuss the transport properties in mechanically deformed polymer networks. First, we present the results for networks under normal stress (Figure 6) and then we probe the effect of shear on the network permeability and self-diffusivity (Figure 7). We normalize the transport coefficients by their corresponding values for unstressed networks and average the relative quantities over 18 realizations. The error bars in Figures 6 and 7 represent the standard deviation from the mean value at each point. The diffusivities in the  $x$ ,  $y$ , and  $z$  directions are calculated by replacing the total displacement  $|\mathbf{r}(t) - \mathbf{r}(0)|$  in the Einstein relation with the displacement in the corresponding coordinate

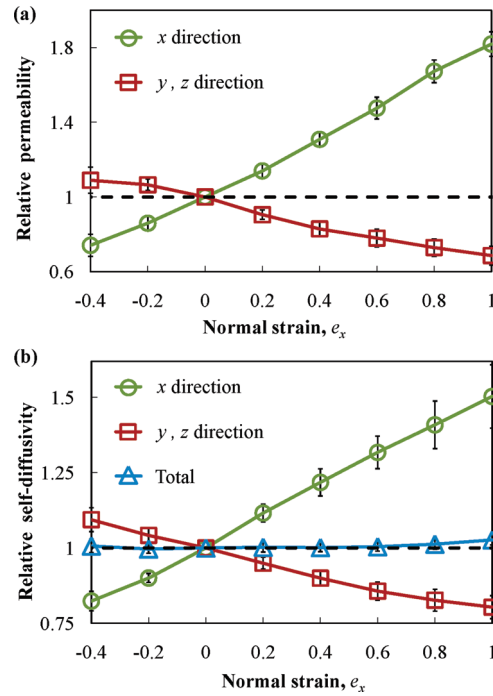


**Figure 6.** (a) Relative permeability and (b) self-diffusivity in the direction of coordinate axes  $xyz$  (see Figure 2) as a function of applied normal strain. The dashed horizontal lines indicate the unity values for unstressed networks. The error bars represent standard deviation from the average over 18 networks with  $N = 250, 500, 1000$  and  $C_{ave} = 4, 6, 8, 10, 12, 14$ .

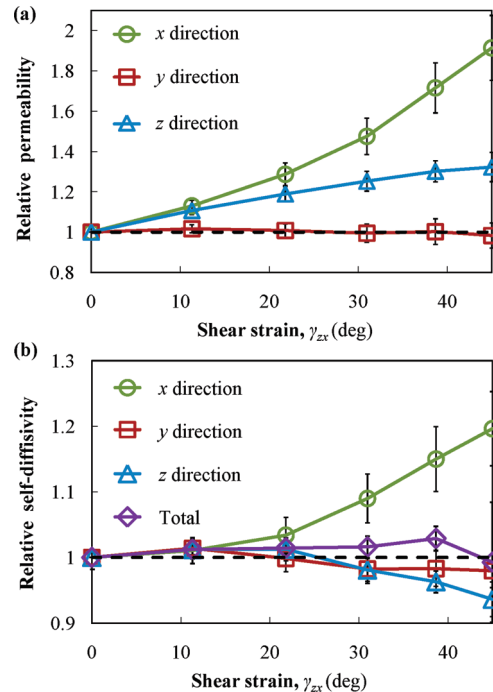


**Figure 7.** (a) Relative permeability and (b) self-diffusivity in the direction of coordinate axes  $xyz$  (see Figure 2) as a function of applied shear strain. The dashed horizontal lines indicate the unity values for unstressed networks. The error bars represent standard deviation from the average over 18 different networks with  $N = 250, 500, 1000$  and  $C_{ave} = 4, 6, 8, 10, 12, 14$ .

directions. Unless specified otherwise, all strains are engineering strains and the network Poisson ratio is 0.5, i.e. the porosity in deformed networks remains unchanged.

Parts a and b of Figure 6 show, respectively, the variation of permeability and self-diffusivity as a function of the normal strain  $e_x$ . The transport coefficients are calculated in the direction of applied stress and in the transverse direction (see Figure 2). In all cases, stretching enhances transport in the elongated direction and hinders it in the transverse direction in which the network is contracted. This phenomenon is a consequence of the change in average orientation of the filaments, which tend to become aligned in the direction of network tension. This anisotropy in filament orientation results in an enhanced transport along aligned filaments. This transport enhancement takes place due to a lower drag experienced by filaments<sup>28</sup> and due to the fact that diffusive objects less likely collide with network filaments in their random walk in the direction of alignment.<sup>23</sup> We find that when the strain exceeds a value of about 5, the network becomes fully aligned and the transport properties no longer change with an additional increase in the strain (provided that the porosity remains unchanged). We also find that the total self-diffusivity remains constant indicating that the net diffusivity only depends on the network porosity which remains unchanged under load.

Under shear, filament orientation changes primarily due to rotation of filaments without a significant change in their overall length. Figure 7 illustrates the changes in relative permeability and self-diffusivity caused by the applied shear strain  $\gamma_{zx}$ . While both permeability and self-diffusion increase in the  $x$  direction with increasing  $\gamma_{zx}$ , they are roughly constant in the  $y$  direction. Furthermore, unlike self-diffusion that slightly decreases in the  $z$  direction, permeability in this direction increases under shear. Also, similar to the axial deformation case, the total self-diffusion remains roughly constant. The application of shear strain only affects the orientation of filaments in the  $xz$  plane. Therefore, the permeability in the  $y$  direction does not change because the in-plane rotation of filaments does not affect the permeability in the direction normal to this plane.<sup>30</sup>

To get a better insight into the deformation-dependent transport properties in random polymer networks, we quantify the mechanical deformation of a network. In our study, the network porosity is invariable under external loads; hence deformation imposed on the network can be translated to changes in the network alignment. To characterize the degree of network alignment, we employ a symmetric second-order orientation tensor<sup>28</sup>

$$\Omega = \frac{1}{l_{total}} \sum l_i \times \begin{bmatrix} \sin^2 \varphi_i \cos^2 \theta_i & \sin^2 \varphi_i \sin \theta_i \cos \theta_i & \cos \varphi_i \sin \varphi_i \cos \theta_i \\ \sin^2 \varphi_i \sin \theta_i \cos \theta_i & \sin^2 \varphi_i \sin^2 \theta_i & \cos \varphi_i \sin \varphi_i \sin \theta_i \\ \cos \varphi_i \sin \varphi_i \cos \theta_i & \cos \varphi_i \sin \varphi_i \sin \theta_i & \cos^2 \varphi_i \end{bmatrix} \quad (1)$$

where  $l_i$  is the length of  $i$ th spring,  $l_{total}$  is the total spring length, and the sum runs over all springs constituting the filaments. Moreover,  $\varphi$  and  $\theta$  are angles between the vector representing the direction of a spring and the  $z$  and  $x$  axis, respectively. The trace of  $\Omega$  is equal to 1 and for isotropic networks  $\Omega_{xx} = \Omega_{yy} = \Omega_{zz} = 1/3$ .<sup>28</sup> When off-diagonal tensor elements are equal to zero, diagonal elements of the orientation tensor characterize the network alignment along the coordinate axes. On the other hand, nonzero off-diagonal components indicate that the network alignment does not coincide with the directions of the coordinate system.

Figure 8 shows how the magnitude of non-zero orientation tensor components changes when the network undergoes mechanical deformation. When a normal force is applied in the  $x$  direction,  $\Omega_{xx}$  increases, and  $\Omega_{yy}$  and  $\Omega_{zz}$  decrease with increasing  $e_x$  (Figure 8a). In addition, the off-diagonal components remain zero, which means that the coordinate axes coincide with the principal directions of the deformed network. When the network

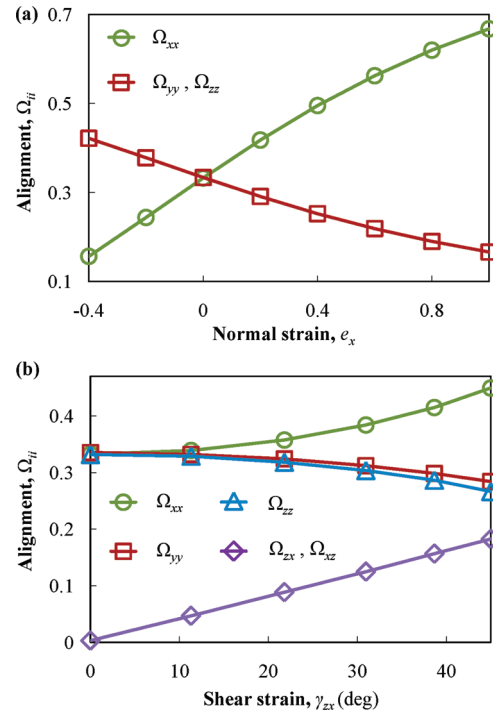


**Figure 8.** Components of a network orientation tensor versus applied (a) normal strain and (b) shear strain. Results are averaged over 18 different networks with  $N = 250, 500, 1000$  and  $C_{ave} = 4, 6, 8, 10, 12, 14$ .

deformation is due to a shearing force (Figure 8b),  $\Omega_{xx}$  increases, while  $\Omega_{yy}$  and  $\Omega_{zz}$  slightly decrease with increasing  $\gamma_{zx}$ . More importantly,  $\Omega_{zx} = \Omega_{xz}$  are not zero and increase with increasing  $\gamma_{zx}$ , indicating that the principal directions of this orientation tensor differ from the directions of the coordinate system  $xyz$  (Figure 2). By rotating the  $xyz$  system along the  $y$ -axis, the tensor can be readily expressed in terms of a new coordinate system  $XYZ$  in which the axes coincide with the principal directions and all off-diagonal elements vanish.

To establish the dependence between the change in transport coefficients and the alignment of the network represented by  $\Omega$ , we transform the  $xyz$  coordinate system to the  $XYZ$  system and plot the relative permeability along the new coordinate directions as a function of the corresponding diagonal components of the transformed orientation tensor (Figure 9). Here, we normalize tensor components by  $\Omega_{iso} = 1/3$ . We find that all data for permeability collapses into a single master curve, which exhibits nearly linear dependence on the magnitude of the orientation tensor eigenvalues (diagonal components in the  $XYZ$ ). We note that the effect of porosity is factored out by averaging the results over 18 different realizations.

Thus, the alignment of network fibers due to an external mechanical load uniquely defines the change of permeability in a given direction relative to the undeformed network. This information can be used to estimate the permeability of polymer networks based on the values of a deformation tensor that can be measured experimentally using 3D imaging techniques.<sup>45,46</sup> Furthermore, we expect that this approach can be extended to assess diffusivity in polymer networks under mechanical load.

## Summary

We developed a hybrid mesoscopic simulation technique to study the permeation and hindered diffusion through isotropic (unstressed) and anisotropic (mechanically loaded) random polymer networks. We validated the model by comparing our results with data from the literature for unstressed networks. In particular,

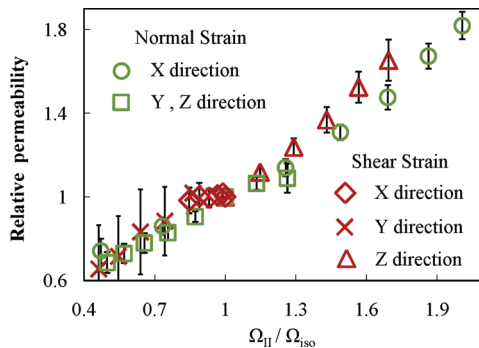


**Figure 9.** Permeability versus degree of alignment in principal directions for networks under normal and shear deformations. The error bars represent standard deviation from the average over 18 different networks with  $N = 250, 500, 1000$  and  $C_{ave} = 4, 6, 8, 10, 12, 14$ .

we found that our simulations compare favorably with the hydrodynamic scaling model for diffusion of rigid particles and linear macromolecules in random networks. We showed that nanoparticles and polymers with similar characteristic sizes exhibit different diffusion rates in unstressed random networks. Specifically, polymers diffuse faster due to their ability to change conformation and deform in the presence of a network.

We found that the network transport properties are defined by network porosity and filament alignment within the network. The network alignment that takes place due to mechanical stretching/compressing or shearing is characterized by a second order orientation tensor. We demonstrated that permeability along the principal directions of a deformed network is directly related to the magnitudes of the corresponding tensor components. Since the orientation tensor can be measured experimentally, this approach opens a way for estimating the permeability of deformable random networks under load.

Our findings are useful for a better understanding of the mechanical properties and dynamic behavior of systems involving synthetic gels and biological polymer networks. In particular, the relation between permeability and network deformability may help to understand the complex lubrication properties of soft rubbing surfaces in synthetic and natural systems, where the dynamic deformations occur as a result of surface interactions.<sup>47,48</sup> Furthermore, the information regarding the particle and chain diffusion in polymer networks can be harnessed to optimize drug delivery systems, including therapeutic agents that penetrate into tumor interstitial matrix to target cancer cells.<sup>49</sup>

**Acknowledgment.** Financial support from the Donors of the Petroleum Research Fund, administered by the ACS, is gratefully acknowledged.

## References and Notes

- (1) Patrickios, C. S. *Macromol. Symp.* **2010**, *291–292* (1), 1–11.
- (2) Liu, L.; Li, P. S.; Asher, S. A. *Nature* **1999**, *397* (6715), 141–144.
- (3) Koenderink, G. H.; Dogic, Z.; Nakamura, F.; Bendix, P. M.; MacKintosh, F. C.; Hartwig, J. H.; Stossel, T. P.; Weitz, D. A. *Proc. Natl. Acad. Sci. U.S.A.* **2009**, *106* (36), 15192–15197.
- (4) Olsson, R. T.; Azizi Samir, M. A. S.; Salazar Alvarez, G.; Belova, L.; Strom, V.; Berglund, L. A.; Ikkala, O.; Nogues, J.; Gedde, U. W. *Nature Nanotechnol.* **2010**, *5* (8), 584–588.
- (5) Saltzman, W. M.; Radomsky, M. L.; Whaley, K. J.; Cone, R. A. *Biophys. J.* **1994**, *66* (2), 508–515.
- (6) Cu, Y.; Saltzman, W. M. *Adv. Drug Delivery Rev.* **2009**, *61* (2), 101–114.
- (7) Durbin, E. W.; Buxton, G. A. *Soft Matter* **2010**, *6* (4), 762–767.
- (8) Park, N.; Um, S. H.; Funabashi, H.; Xu, J.; Luo, D. *Nat. Mater.* **2009**, *8* (5), 432–437.
- (9) Chen, X. M.; Dunn, A. C.; Sawyer, W. G.; Sarntinoranont, M. *J. Biomech. Eng.-T. Asme* **2007**, *129* (2), 156–163.
- (10) Hutmacher, D. W. *Nat. Mater.* **2010**, *9* (2), 90–93.
- (11) Murase, Y.; Maeda, S.; Hashimoto, S.; Yoshida, R. *Langmuir* **2009**, *25* (1), 483–489.
- (12) Dayal, P.; Kuksenok, O.; Balazs, A. C. *Soft Matter* **2010**, *6* (4), 768–773.
- (13) Shingo, M.; Hara, Y.; Yoshida, R.; Hashimoto, S. In *Chemical robot-Design of self-walking gel-*; IROS 2007. IEEE/RSJ International Conference on Intelligent Robots and Systems, Oct. 29 2007–Nov. 2 2007; **2007**; pp 2150–2155.
- (14) Daganl, R. *Chem. Eng. News* **1997**, *75* (23), 26–37.
- (15) Barbucci, R.; Ratner, B. D.; Atzet, S. Hydrogels for Healing. In *Hydrogels*; Springer: Milan, 2009; pp 43–51.
- (16) Spielman, L.; Goren, S. L. *Environ. Sci. Technol.* **1968**, *2* (4), 279–287.
- (17) Mansour, J. M.; Mow, V. C. *J. Bone Joint Surg. Am.* **1976**, *58* (4), 509–516.
- (18) Jackson, G. W.; James, D. F. *Can. J. Chem. Eng.* **1986**, *64* (3), 364–374.
- (19) Whitaker, S. *Transport Porous Media* **1986**, *1* (1), 3–25.
- (20) Phillips, G. D. *J. Phys. Chem.* **1989**, *93* (13), 5029–5039.
- (21) Phillips, G. D. J.; Pirnat, T.; Kiss, M.; Teasdale, N.; Maclung, D.; Inglefield, H.; Malone, C.; Rau, A.; Yu, L. P.; Rollings, J. *Macromolecules* **1989**, *22* (10), 4068–4075.
- (22) Clague, D. S.; Phillips, R. *J. Phys. Fluids* **1997**, *9* (6), 1562–1572.
- (23) Bosma, J. C.; Wesselingh, J. A. *J. Chromatogr. B* **2000**, *743* (1–2), 169–180.
- (24) Gu, W. Y.; Yao, H.; Huang, C. Y.; Cheung, H. S. *J. Biomech.* **2003**, *36* (4), 593–598.
- (25) Markert, B. *Transport Porous Media* **2007**, *70* (3), 427–450.
- (26) Mu, D.; Liu, Z. S.; Huang, C.; Djilali, N. *Microfluid Nanofluid* **2008**, *4* (3), 257–260.
- (27) Seiffert, S.; Oppermann, W. *Polymer* **2008**, *49* (19), 4115–4126.
- (28) Stylianopoulos, T.; Yeckel, A.; Derby, J. J.; Luo, X. J.; Shephard, M. S.; Sander, E. A.; Barocas, V. H. *Phys. Fluids* **2008**, *20* (12), 123601.
- (29) Nabovati, A.; Llewellyn, E. W.; Sousa, A. C. M. *Compos. Part a: Appl. Sci.* **2009**, *40* (6–7), 860–869.
- (30) Tahir, M. A.; Tafreshi, H. V. *Phys. Fluids* **2009**, *21* (8), 083604.
- (31) Chandran, P. L.; Stylianopoulos, T.; Barocas, V. H. *Multiscale Model Simul.* **2008**, *7* (1), 22–43.
- (32) Buxton, G. A. *EPL* **2008**, *84* (2), 26006.
- (33) Hoogerbrugge, P. J.; Koelman, J. M. V. A. *Europhys. Lett.* **1992**, *19* (3), 155–160.
- (34) Groot, R. D.; Warren, P. B. *J. Chem. Phys.* **1997**, *107* (11), 4423–4435.
- (35) Groot, R. D.; Rabone, K. L. *Biophys. J.* **2001**, *81* (2), 725–736.
- (36) Chen, S.; Phan-Thien, N.; Fan, X. J.; Khoo, B. C. *J Non-Newton Fluid* **2004**, *118* (1), 65–81.
- (37) Alexeev, A.; Upfal, W. E.; Balazs, A. C. *ACS Nano* **2008**, *2* (6), 1117–1122.
- (38) Fedosov, D. A.; Karniadakis, G. E.; Caswell, B. *J. Chem. Phys.* **2008**, *128* (14), 144903.
- (39) Masoud, H.; Alexeev, A. *Chem. Commun.* **2011**, DOI: 10.1039/C0CC02165B.
- (40) Espanol, P.; Warren, P. *Europhys. Lett.* **1995**, *30* (4), 191–196.
- (41) Fan, X. J.; Phan-Thien, N.; Chen, S.; Wu, X. H.; Ng, T. Y. *Phys. Fluids* **2006**, *18* (6), 063102.
- (42) Pan, W. X.; Fedosov, D. A.; Karniadakis, G. E.; Caswell, B. *Phys. Rev. E* **2008**, *78* (4), 46706.
- (43) Buxton, G. A.; Clarke, N. *Phys. Rev. Lett.* **2007**, *98* (23), 238103.
- (44) Kasper, G.; Niida, T.; Yang, M. *J. Aerosol Sci.* **1985**, *16* (6), 535–556.
- (45) Mickel, W.; Munster, S.; Jawerth, L. M.; Vader, D. A.; Weitz, D. A.; Sheppard, A. P.; Mecke, K.; Fabry, B.; Schroder-Turk, G. E. *Biophys. J.* **2008**, *95* (12), 6072–6080.
- (46) Kotlarchyk, M. A.; et al. *J. Phys.: Condens. Matter* **2010**, *22* (19), 194121.
- (47) Gong, J. P. *Soft Matter* **2006**, *2* (7), 544–552.
- (48) Chang, D. P.; Dolbow, J. E.; Zauscher, S. *Langmuir* **2007**, *23* (1), 250–257.
- (49) Ramanujan, S.; Pluen, A.; McKee, T. D.; Brown, E. B.; Boucher, Y.; Jain, R. K. *Biophys. J.* **2002**, *83* (3), 1650–1660.